Biochimica et Biophysica Acta 850 (1986) 324–332
Elsevier

BBA 42043

The state of manganese in the photosynthetic apparatus. 4. Structure of the manganese complex in Photosystem II studied using EXAFS spectroscopy. The S_1 state of the O_2-evolving Photosystem II complex from spinach *

Vittal K. Yachandra, R.D. Guiles, Ann McDermott, R. David Britt, S.L. Dexheimer, Kenneth Sauer and Melvin P. Klein **

Laboratory of Chemical Biodynamics, Lawrence Berkeley Laboratory, University of California, Berkeley, CA 94720 (U.S.A.)

(Received October 29th, 1985)
(Revised manuscript received March 12th, 1986)

Key words: Oxygen evolution; Manganese; EXAFS; Photosystem II; (Spinach chloroplast)

The structure of the Mn complex in the oxygen-evolving system and its mechanistic relation to photosynthetic oxygen evolution are poorly understood, though many studies have established that membrane-bound Mn plays an active role. Recently established procedures for isolating oxygen-evolving subchloroplast Photosystem II (PS II) preparations and the discovery of a light-induced multiline EPR signal attributable to the S_2 state of the O_2-evolving complex have facilitated the preparation of samples well characterized in the S_1 and S_2 states. We have used extended X-ray absorption fine structure (EXAFS) spectroscopy to probe the ligand environment of Mn in PS II particles from spinach, and in this report we present our results. The essential feature of the EXAFS results are that at least two Mn atoms per PS II reaction center occur as a binuclear species with a metal–metal distance of approx. 2.7 Å, with low Z atoms, N or O, at a distance of approx. 1.75 Å and at approx. 1.98 Å, which are characteristic of bridging and terminal ligands. These results agree well with those derived from whole chloroplasts that provided the first evidence for a binuclear manganese complex (Kirby, J.A., Robertson, A.S., Smith, J.P., Thompson, A.C., Cooper, S.R. and Klein, M.P. (1981) J. Am. Chem. Soc. 103, 5529–5537).

Introduction

The oxidation of water to molecular oxygen in algae and higher plants involves the stepwise transfer of oxidizing equivalents by the Photosystem II reaction center. The oxidizing potential produced by the photosynthetic charge separation is stored at or near the site of water oxidation in a membrane-bound complex that contains manganese [1]. Though extensive studies over the past few decades have shown that manganese, Cl^- and PS II are somehow involved in this water-oxidation reaction, the mechanism of the reaction or the structure of the manganese-containing oxygen-evolving complex is poorly understood [2].

Kinetic studies of the O_2 produced by pulses of

* This paper is dedicated to the memory of Dr. Jon Kirby.
** To whom correspondence should be addressed.
Abbreviations: AcAc, acetylacetonate; Chl, chlorophyll; DMBQ, 2,6-dimethyl-*p*-benzoquinone; EXAFS, extended X-ray absorption fine structure; Hepes, 4-(2-hydroxyethyl)-1-piperazineethanesulfonic acid; Mes, 4-morpholineethanesulfonic acid; PMSF, *p*-toluene sulfonylfluoride; PS, Photosystem; TPP, tetraphenylporphyrin.

saturating light have given rise to a model for the accumulation of oxidizing equivalents in which five intermediates S_0–S_4 operate in a cyclic fashion [3]. The identity of the S intermediates has not been established, but evidence implicates a form of membrane-bound manganese. Manganese-deficient algae do not evolve O_2, and the inability can be overcome by the addition of Mn to deficient cells [4]. More recently the evidence for the association of manganese with the S state intermediates has emerged from the observation at low temperature of a complex EPR signal in illuminated spinach chloroplasts [5–7], which is similar to that observed in a model dimeric Mn species [8]. The flash dependence of the multiline EPR signal led Siderer and Dismukes [5] to assign the signal to the S_2 state of the O_2-evolving complex. The temperature dependence of the light-induced formation and subsequent decay of the signal also indicates that it is correlated with the presence of the S_2 state of the O_2-evolving complex [9]. Treatments that affect O_2 evolution, including alkaline Tris washing, cause the disappearance of this signal and the apparent release of Mn to a form that is EPR detectable at room temperature [10].

We have recently reported the light-induced changes in the X-ray Mn K-edge spectra from PS II particles using the low temperature multiline EPR signal as an indicator of the S state composition [11,12]. This is direct evidence that the membrane-associated Mn atoms participate in the light-driven storage of oxidizing equivalents at the PS II oxygen-evolving complex.

Our previous results [13] indicative of a binuclear manganese structure in the oxygen-evolving complex were obtained from difference EXAFS studies using whole chloroplasts. Broken washed chloroplast preparations typically contain 4–6 Mn/PS II reaction center, and approx. 2/3 of this quantity is released by treatments that specifically inhibit O_2 evolution, such as alkaline Tris washing, mild thermal shock or high salt incubation [14]. Our approach was to use difference EXAFS (active-minus-Tris-inactivated pool) to obtain the structure of the active Mn pool. More recently, the development of Photosystem II sub-chloroplast preparations that are more homogeneous in manganese content has simplified the data analysis and interpretation of the EXAFS results, without requiring recourse to difficult difference EXAFS studies.

We have completed the EXAFS measurements, which provide a good method for determining the nature of the ligands and the distances at which they are bound to the central absorbing atom [15–17]. EXAFS is element-specific and hence well suited for situations where the metallo-enzyme cannot be isolated to purity or cannot be separated from the organelle matrix. Few other spectroscopic tools provide such specificity on the structure of the Mn complex in the photosynthetic apparatus. In this report we present the EXAFS results from the S_1 state of the PS II oxygen-evolving complex using spinach PS II particles.

The requirement for Cl^- on the donor side of PS II [18,19] and its involvement with the Mn containing complex has been established [20–23], and models have been presented suggesting that Cl^- ion could be ligated to Mn [19,24]. Since Br^- ion is an effective replacement for Cl^- ion we have looked for differences in the high resolution EPR multiline spectrum in Cl^- and Br^- containing PS II particles. Our studies indicate no variations in the fine structure of the EPR spectrum, suggesting that the halide ion is not involved in the first coordination sphere of the EPR active Mn complex [25]. We interpret our EXAFS results to arrive at a chemical model, which also addresses the question of halide ligation.

Materials and Methods

Preparation of O_2-evolving PS II sub-chloroplast membranes was accomplished by a modification of two different Triton X-100 fractionation procedures [26,27]. Broken chloroplasts were prepared from destemmed fresh market spinach by grinding in a Waring blender for 10–15 s at 4°C in a medium containing 20 mM Hepes (pH 7.5)/0.4 M NaCl/2 mM $MgCl_2$/1 mM EDTA/50–100 μM PMSF. The homogenate was strained through eight layers of cheesecloth and centrifuged at 4°C for 10 min at $6000 \times g$. The pellet was suspended in 0.15 M NaCl/4 mM $MgCl_2$/20 mM Hepes (pH 7.5) and spun at $6000 \times g$ for 10 min. We have found that it is important to complete the procedure from grinding to the washing stage within 30 min. The pellet was resuspended in a

buffer containing 50 mM Hepes (pH 7.5)/0.4 M sucrose/10 mM NaCl/1 mM $MgCl_2$ and filtered through four layers of miracloth. The filtrate was then spun at $100 \times g$ for 30 s, the loose pellet discarded and the broken chloroplasts pelleted by a 10 min spin at $6000 \times g$.

The pellet was suspended in 50 mM Mes (pH 6.0)/15 mM NaCl/5 mM $MgCl_2$/1 mM sodium ascorbate to a concentration of 2 mg per ml Chl. Triton X-100 25% in Mes buffer was added with vigorous stirring to give a Triton X-100-to-Chl ratio of 25 : 1 (w/w). After incubation in the dark for 1 min the suspension was spun at $100 \times g$ for 2 min. The pellet was discarded and the supernatant was centrifuged at $35000 \times g$ for 10 min. The pellet was resuspended in 50 mM Mes (pH 6.0)/10 mM NaCl/5 mM $MgCl_2$ and the loose pellet, after a $1000 \times g$ spin was discarded, and the PS II sub-chloroplast membranes were pelleted by centrifugation at $35000 \times g$ for 10 min.

The pellet was washed once more in the suspension buffer containing 50 mM Mes (pH 6.0)/10 mM NaCl/5 mM $MgCl_2$ and then spun at 35000 $\times g$ for 1 h to give tightly packed PS II particles. The samples for X-ray absorption studies were about 20–30 mg per ml Chl and contained approx. 30% glycerol. The Mn concentration as measured by atomic absorption spectroscopy was 4–5 Mn atoms/250 Chl. O_2 evolution rates of 300–400 μmol O_2 per mg Chl per h were assayed in suspension buffer containing 50 mM Mes (pH 6.0)/10 mM NaCl/5 mM $MgCl_2$/500 μM DMBQ/1 mM $K_3Fe(CN)_6$/1 mM $K_4Fe(CN)_6$.

The samples were dark adapted for 2 h at 4°C, equilibrated at 190 K in a Varian V 6040 NMR temperature controller and illuminated with a 400 W tungsten lamp through a 5 cm water filter. The samples were again dark adapted for 2 h at 4°C and then frozen in liquid nitrogen. This preillumination was given to decrease the S_0 concentration, which would otherwise constitute 25% of O_2-evolving complex centers [3].

The EXAFS samples were mounted in lucite sample holders, with a sample area of 4 cm × 4 mm for incidence of the whole X-ray beam upon the sample material. The samples were supported on the distal side by mylar film. The size of the sample holders was so chosen that they could also be inserted directly into an Air products Helitran cryostat for monitoring of the EPR spectrum of the sample.

To ensure the functional and structural integrity of the samples we monitored the EPR spectra using a Varian E9 at approx. 8 K, before and after X-ray exposure. No multiline EPR signal characteristic of the S_2 state was observed in the S_1 samples before or after X-ray exposure, confirming that the sample was mostly in the S_1 state. The O_2 activity was also assayed before and after X-ray exposure and no significant changes were observed, ensuring that radiation damage to the functional O_2 evolving centers was minimal.

The Mn compounds Mn(II)$(AcAc)_2$, Mn(III)$(AcAc)_3$, and Mn(IV)O_2 were obtained commercially and Mn(III,IV)bipyridyl dimer was synthesized following the published procedure [8].

X-ray measurements and data analysis

X-ray absorption spectra were obtained at the Stanford Synchrotron Radiation Laboratory, Stanford, CA during dedicated operation of the SPEAR storage ring, providing 40–80 mA electron beams at 3.0 GeV. The Mn EXAFS spectra were obtained in fluorescence mode [28] on the 54 pole wiggler beam line (VI-2, SSRL/EXXON/LBL beam line). The focused X-ray beam provided fluxes of approx. $1 \cdot 10^{13}$ photons $\cdot s^{-1} \cdot$ mrad$^{-1} \cdot$ eV^{-1} with about 1 eV resolution when equipped with a Si⟨400⟩ double crystal monochromator.

The samples contained in lucite holders were inserted in a temperature regulated cryostat in darkness, maintained at 170 K. At 170 K it has been determined that radiation damage is minimal; it is also a temperature where the S state system cannot advance beyond the S_1 state. The cryostat was fabricated in our laboratory. It consisted of a sample chamber which was insulated from the outside by two layers of Kapton. The sample temperature was regulated by controlling the flow of cooled N_2 boil off. Dry N_2 gas was circulated through the space between the layers of Kapton to inhibit frost formation, and air blowers were used on the outside to prevent water condensation on the cryostat.

The incident intensity, I_0, of the X-ray beam was monitored by an ionization chamber and, F, the Mn X-ray K-edge fluorescence was measured

using a plastic scintillation array similar to that described by Powers et al. [29]. The scintillation counters were constructed by attaching NE 104 plastic scintillator (Nuclear Enterprises, 5.08 cm in diameter and 2.54 cm thick) to a EMI 9813B eleven stage photomultiplier (EMI Gencom). Spectral response of the tube was maximal at the wavelength appropriate to the scintillator emission. The assembly was mounted in a light–tight tubular housing and protected from ambient light by two layers of 0.025 mm thick aluminized mylar film. Seven such counters were mounted in an array and approximately equidistant from the sample. The entire assembly was equipped with a Soller slit assembly and with Cr fluorescence filters, which consisted of 0.25 mm thick Be with Cr electrodeposited to a thickness of 0.013 mm [30]. To reduce extraneous scattered radiation from reaching the detector, a lead tape shielding was used around the detector assembly. The signal from each photomultiplier was passed through a constant fraction discriminator, and the output from each channel was stored in a Digital PDP 11/34 computer.

The data were analyzed as described in detail elsewhere [13,31] and only a brief summary will be presented here. For EXAFS analysis, many single scans were added after they were examined for satisfactory S/N, edge energy and absence of anomalies. Monochromator settings were converted to X-ray energy, and a linear background which set absorption prior to the edge to zero was subtracted from the averaged data.

The EXAFS modulation of the absorption is given by the equation:

$$\chi(k) = \sum_i \frac{N_i f_i(k, \pi)}{kR_i^2} e^{-2R_i/\lambda(k)} e^{-2\sigma^2(k)k^2} \times \sin\{2kR_i + \alpha_i(k)\}$$

where N_i is the number of the ith type of backscattering atoms at R_i, $\lambda(k)$ is the photoelectron mean free path, and $f_i(k, \pi)$ is the backscattering amplitude of the ith atom (which is approx. Z/k^2, for $k > 4.0$ Å^{-1}, Z is the atomic number of backscattering atom), $\sigma^2(k)$ is the Debye-Waller factor describing the mean square displacement in R_i (from thermal and static disorder), $\alpha_i(k)$ is the energy-dependent phase shift of the photoelectron caused by the potentials of both the absorbing and the backscattering atom, k is the magnitude of the photoelectron wave-vector given by

$$k = \frac{\{2m_e(E - E_0)\}^{1/2}}{\hbar}$$

where m_e is the electron mass, E is the X-ray energy and E_0 is the edge energy [15–17].

The EXAFS modulation $\chi(k)$ was extracted from the data by subtracting a cubic spline fit to remove the isolated atom or background contribution and normalized to one absorbing atom by the magnitude of the edge. Generally, $\chi(k)$ is multiplied by k^3 to compensate for the $1/k^3$ dependence of $\chi(k)$. However, this also increases the noise of the data at higher energies. Because we are dealing with a very dilute system (Mn concentration of approx. 500–800 μM) and the S/N ratio is relatively small, we chose to multiply our data by k^1. Fourier transformation of the background-subtracted data produces a radial distribution of photoelectron backscattering as a function of apparent distance $R' = R + \frac{1}{2}\alpha(k)$ where R is the true distance from the absorbing atom, and $\alpha(k)$ is the phase shift of the absorber-scatterer pair due to their respective potentials [32,33]. The contribution that each shell makes to the EXAFS was determined by applying a window function prior to back transformation of the individual R'-space feature to k-space. The back-transformed data were then fit by the Teo-Lee method [34], which uses theoretical values for the amplitude and phase functions. The values of the average distance, R, the number of scatterers, N, at distance R, the Debye-Waller factor, σ, and the threshold energy, E_0, are simultaneously fit with a nonlinear least-squares fitting program. The final step is to perform multishell fits on a Fourier-isolated k-space spectrum which includes all of the R space peaks of interest. This method is used to remove the residual low-frequency background and high-frequency noise, thereby greatly improving the precision of the fits.

Results

A representative signal-averaged fluorescence-detected Mn X-ray absorption spectrum is shown

in Fig. 1 for spinach oxygen-evolving PS II particles in the S_1 state. In the k^1-multiplied, background-subtracted EXAFS portion of the data (Fig. 2), it can be seen that the EXAFS modulations are complicated and are characterized by contributions from two or more sinusoidal oscillations. Similar ligand atoms at a unique distance would give rise to a single modulation frequency. The more complex spectrum observed points to a structure with more than one distance or type of scatterer or both.

The contribution of the various scattering shells to the EXAFS spectrum becomes more evident in the Fourier transform of the k-space data, which produces a radial distribution of the photoelectron backscattering, as illustrated in Fig. 3. The peak labelled I at $R' = R + \frac{1}{2}\alpha(k)$ of approx. 1.1 Å is due to the nearest-neighbor atoms (first shell). The second peak labelled II occurs at an R' of approx. 1.6 Å and is from a second shell of ligands. These two Fourier peaks occur at distances from Mn characteristic for bridging and terminal N or O ligands in μ-oxo bridged binuclear Mn clusters [35]. The third Fourier peak III at R' of approx. 2.2. Å is characteristic of a scattering contribution from a transition metal, in this case probably another Mn atom [35]. Note the real distances are larger than R' by $\alpha/2$, because α is less than zero.

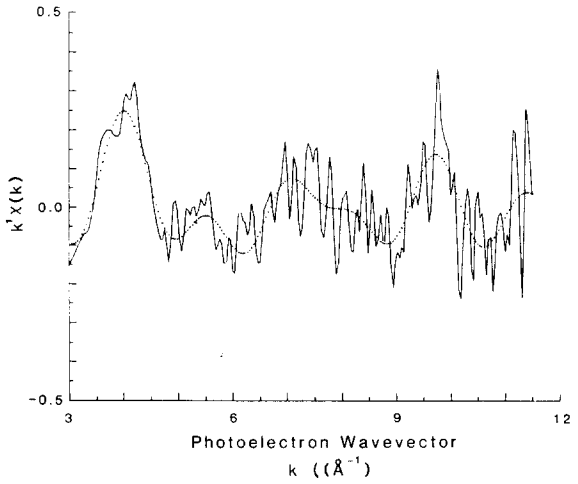

Fig. 2. Background-removed Mn EXAFS data $\chi(k)$, multiplied by k^1 and normalized to unit edge rise by extrapolation of the smooth free-atom background, is plotted as a function of the photoelectron wave-vector k. The dotted line is the Fourier-filtered curve.

The Fourier peaks at larger distances (more than 3.0 Å) may be due to scattering from further coordination shells. Previously such shells have

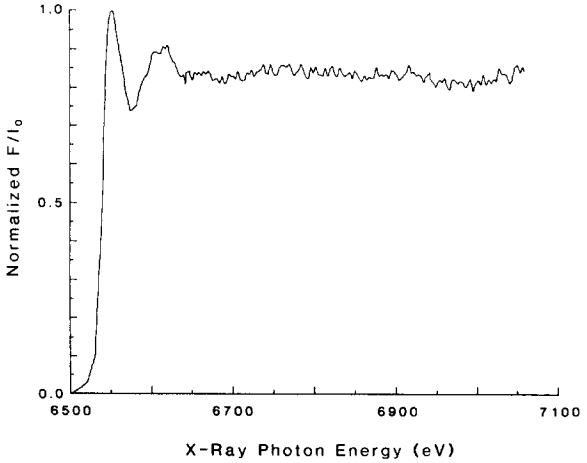

Fig. 1. X-ray absorption spectrum of Mn in PS II particles from spinach in the S_1 state. A smooth background has been removed, which sets absorption prior to the edge to zero. Data were collected by fluorescence F, and I_0 is the incident intensity. Normalized F/I_0 is plotted as a function of X-ray photon energy in eV.

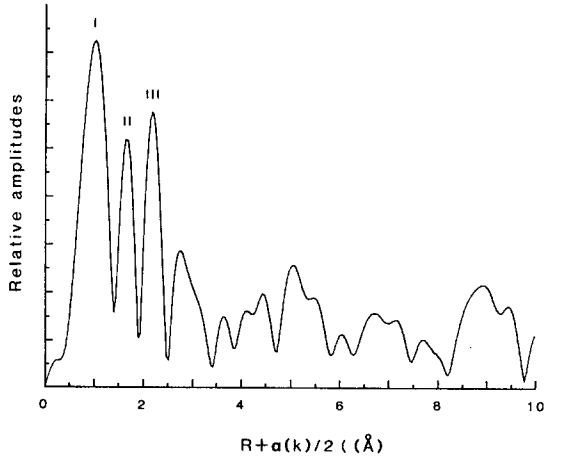

Fig. 3. Fourier transform of the $k^1\chi(k)$ data of Mn in the S_1 state. The Fourier transform is for the data set from $k = 3.0$ to 11.5 Å. Note that the amplitude of the transform is plotted as a function of $R' = R + \frac{1}{2}\alpha(k)$, where R is the distance of the scattering atom from Mn and $\frac{1}{2}\alpha(k)$ is the phase shift of the absorber-scatterer pair due to their respective potentials.

been observed in metal-imidazole and metal-histidine complexes, where they were attributed to the C atoms of the imidazole rings [36,37]. The signal-to-noise of our data precludes any such definitive assignments at this time.

We also examined the Fourier transform of the k^3-multiplied EXAFS data (not shown). The purpose in examining k^3 transforms is to support our identification of the scattering elements. Theoretical backscattering amplitudes obtained by Teo and Lee [34] show that as the atomic number increases (1) the maximum point of the backscattering cross section moves to higher k values and (2) the total backscattering capability increases. These characteristics imply that if two different atoms are at the same distance, then the heavier one will backscatter more efficiently at higher k and if the EXAFS spectrum is multiplied by k^3 then the transform peak of a heavier atom will be preferentially enhanced. This behaviour usually permits the transform peaks of the heavier atoms to be identified. This method of analysis supports our conclusions that peak III in the Fourier transform is due to a transition metal (in this case probably an Mn atom) and the Fourier peaks I and II are from low Z scatterers like N or O atoms [38].

Fig. 4 shows the Fourier-filtered EXAFS modulations associated with the three Fourier peaks I, II and III. These filtered data were fit to phase and amplitude functions obtained from theoretical calculations by the method of Teo and Lee, and the best fit is superimposed on the data.

The best fit parameters are that each Mn atom is coordinated to 3.25 N or O ligand atoms at a distance of 1.98 Å, 2.27 O or N ligand atoms at 1.75 Å and to 0.68 Mn atoms at a distance of 2.69 Å. The uncertainty in R is ± 0.03 Å. Significant correlations exist between N and σ, making the error in N approx. 20%; it can be as high as approx. 50% [39]. However, we emphasize that the uncertainty is mostly in the number of scatterers N; the radial distances, and the identity of the scatterers, nitrogen and oxygen in two shells and Mn in the third shell, are essential for any reasonable fit. The results are summarized in Table I.

Because of the importance of the result regarding the existence of a neighboring Mn atom, we analyzed the peak labelled III separately. The Fourier-filtered backtransformed k-space data are shown in Fig. 5 with the best theoretical fit. The best fit is 0.77 Mn atoms at a distance of 2.67 Å.

Typical Mn–Cl distances in model complexes like ClMn(III)TPP are 2.37 Å [40] and can be as large as 0.247 nm in some complexes [41]. A Cl atom at this distance would give rise to a Fourier

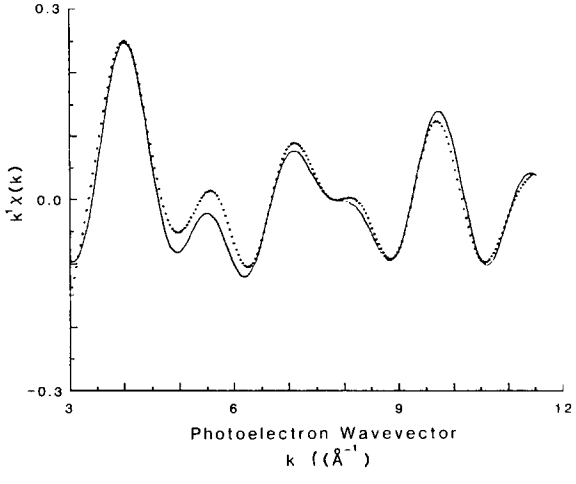

Fig. 4. Fourier filtered EXAFS data from the Fourier peaks labelled I, II and III in Fig. 3. The filter window for the back transform was from R' 0.0 to 2.75 Å. The dotted line is the best fit to the EXAFS data using theoretical phase and amplitude functions derived using the Teo-Lee method [34].

TABLE I

PARAMETERS EXTRACTED FROM THE Mn EXAFS DATA OF PS II PARTICLES IN THE S_1 STATE, ACCORDING TO THE TEO-LEE METHOD

R is the distance from the Mn to the various scatterers ± 0.03 Å. N is the coordination number $\pm 20\%$. ΔE_0 is the difference between the best fit E_0 and the energy at the top of the edge. The Debye-Waller factor σ used in the above simulations was fixed at a value of 0.022 Å. The least-square error weighted by k^1 for the 3-shell fit is 0.075 and for the 1 shell fit is 0.018.

	R (Å)	N	ΔE_0 (eV)
3-shell fit			
I Mn–N or O	1.76	2.27	−5.3
II Mn–N or O	1.98	3.25	−19.9
III Mn–Mn	2.69	0.68	−9.7
1-shell fit			
III Mn–Mn	2.67	0.77	−16.1

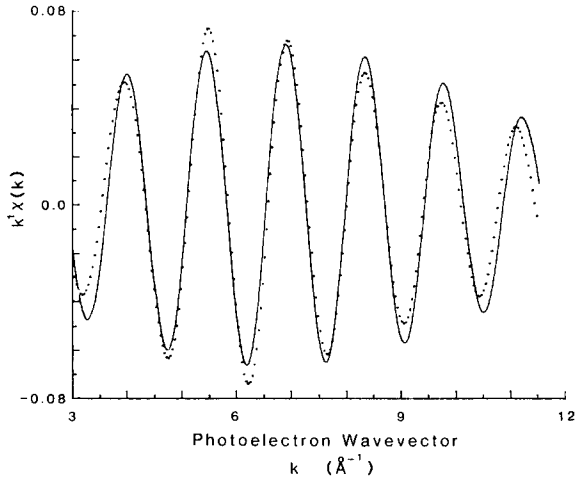

Fig. 5. Fourier filtered Mn EXAFS data from the Fourier peak labelled III in Fig. 3. The Fourier window was from $R' = 1.8$ to 2.75 Å. The dotted line is the best fit to the EXAFS data using curve-fitting techniques explained in the text. The best fit is 0.77 Mn atoms at 2.67 Å nm.

peak at an R' of approx. 0.2 nm. The Fourier transform shown in Fig. 3 is devoid of any such feature. Another alternative that we considered is that Cl exists at an atypical distance in this complex. Accordingly, we tried forcing a fit using Cl phase and amplitude functions; however, we were unable to arrive at any physically resonable parameters. The analysis of the data rules out a model in which any Cl is bound to Mn in the first coordination sphere in the S_1 state.

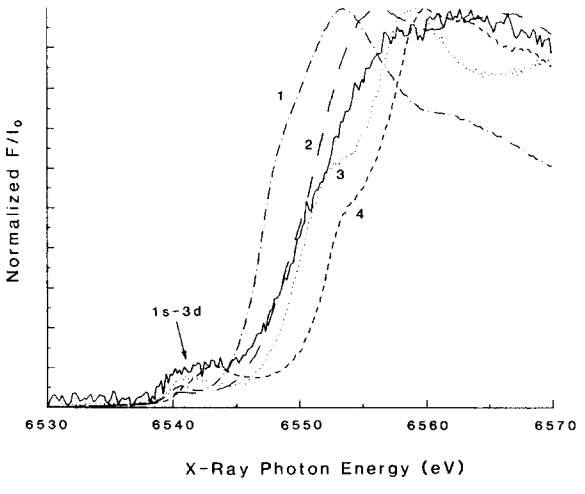

Fig. 6. The solid line is the X-ray absorption Mn K-edge spectra of Mn in spinach PS II particles in the S_1 state. The Mn K-edge inflection is at 6550.4 eV. The small pre-edge absorption at approx. 6543 eV is due to the 1s–3d bound-state transition. The Mn K-edge spectra of (1) ·–·–·, $Mn(AcAc)_2$; (2) — — —, $Mn(III)(AcAc)_3$; (3) ·····, Mn(III,IV)bipyridyl dimer; and (4) - - - - -, $Mn(IV)O_2$ are shown for comparison.

The Mn K-edge spectrum of a spinach PS II preparation in the S_1 state is presented in Fig. 6 (solid line). The dashed lines are the Mn K-edge spectra of model complexes $Mn(II)(AcAc)_2$, $Mn(III)(AcAc)_3$, Mn(III,IV)bipyridyl dimer and $Mn(IV)O_2$ from left to right. The S_1 inflection point lies close to that of the Mn(III) complex. Also a small pre-edge shoulder, which is due to a 1s–3d bound state transition is observed in the S_1 Mn K-edge spectrum.

Discussion

Our deductions of the structure of the Mn complex in PS II oxygen-evolving particles confirm our earlier conclusions based on measurements on intact thylakoids [13]. The results are consistent with a binuclear Mn structure with a Mn–Mn distance of 2.68 Å (average from the three shell and one shell fits), with each Mn coordinated to 3 ± 1 N or O terminal ligands at 1.98 Å and 2 ± 1 N or O bridging ligands at a distance of 1.75 Å. This structure agrees well with our results obtained from whole chloroplast difference EXAFS and closely resembles the published crystal structure parameters for the di-μ-oxo tetrakis(2,2′-bipyridine) dimanganese(III,IV)perchlorate [35].

Preliminary EXAFS results from PS II particles from spinach in the S_2 state and from the thermophilic bacterium *Synechococcus* also indicate a binuclear bridged structure. The results are being prepared for publication.

EPR evidence for the direct involvement of Mn in the S state cycle has been provided by the observation of a light-induced EPR signal at low temperature [5,6]. Based on the hyperfine structure and its similarity to the bipyridyl di-μ-oxo Mn dimer, Dismukes et al. proposed a weakly exchange coupled Mn(III,IV) binuclear or a Mn(III,III,III,IV) tetranuclear cluster [7]. Based on the EXAFS data it is possible to choose between these two alternate structures by directly

measuring the coordination of the Mn atoms in the PS II complex.

However, it is necessary to note that EXAFS data provide a composite measure of the coordination of all of the Mn atoms in the system. Therefore, it is important and pertinent to discuss (1) the homogeneity of the Mn present in the PS II system, (2) whether a multinuclear Mn center exists and, if it does, (3) whether it is binuclear or tetranuclear. Our data for the S_1 state indicate that each Mn atom sees on an average 0.68–0.77 Mn atoms at a distance of 2.68 Å. Considering the uncertainty inherent to the method this suggests that each Mn atom is associated with 0.5–1.0 Mn atoms.

It is generally agreed that the PS II subchloroplast system contains 4 Mn atoms/PS II reaction center assuming 250 Chl per reaction center [42–44]. A tetrameric Mn structure with equidistant Mn centers would give a Mn coordination number of 3.0, which is beyond the limits of the error inherent in our measurements. Possibilities which would be consistent with our data are (A) two equivalent binuclear complexes, which would give an average Mn coordination of 1.0 per Mn atom, or (B) one binuclear complex with 1 or 2 other Mn atoms incorporated as monomers, which would arrive at an Mn coordination of 0.5 or 0.66, both of which are within the limits of the uncertainty of our measurements and analytical procedures.

Our Mn X-ray K-edge data (Fig. 6) show that the Mn K-edge inflection occurs at about 6550.4 eV, which is close to the Mn K-edge of Mn(III) complexes. The Mn(II) oxidation state, which would be the likely oxidation state of non specifically bound Mn, has a K-edge at about 6542–6548 eV [45]. This suggests that most of the Mn is in a specific environment. This conclusion is supported by the presence of the pre-edge feature in the edge spectrum at approx. 6543.0 eV, which is assigned to the 1s–3d transition and is characteristic of non-centrosymmetric complexes [46] or exchange coupled binuclear complexes [47]. It is not observed in non-specifically bound Mn complexes (similar to Mn(II)aqueous) and it is a good indicator that most of the Mn in the PS II particle is in a specialized non-centrosymmetric environment. EXAFS data and the Mn K-edge data can accommodate one binuclear cluster with one or two other Mn atoms with a III or IV oxidation state, and which are further than 0.3 nm from the binuclear cluster or the model consisting of two equivalent Mn binuclear clusters.

Both alternatives are consistent with the recent proposals for two interacting paramagnetic centers, which have been advanced to explain the temperature dependence and power saturation properties of the multiline EPR spectrum [48]. Also, recent absorbance difference studies by Van Gorkom [49] have indicated the requirement for 3 Mn atoms in the S state cycle.

Finally, one of the models proposed to explain the Cl^- effect requires that Cl^- be a ligand to Mn [19,24]. Our EPR studies with Cl^- and Br^- substituted PS II particles have failed to show any such invovlement of the halide in the first coordination sphere of the EPR active Mn in the S_2 state [25]. This is consistent with our EXAFS results, where we find no evidence for Cl binding in the first coordination shell of Mn in the S_1 state. It is possible that the halide is needed for electron transport between two binuclear complexes or between one binuclear complex and another specialized Mn atom; however, the halide must be more than approx. 3.0–4.0 Å from either center.

Acknowledgements

We thank Dr. David Goodin for many useful discussions concerning X-ray fluorescence measurements. This work was supported by a grant from the National Science Foundation (PCM 82-16127 and PCM 84-16676) and by the Director, Office of Energy Research, Office of Basic Energy Sciences, Division of Biological Energy Conversion and Conservation of the Department of Energy under contract DE-AC03-76 SF00098.

References

1 Sauer, K. (1980) Acc. Chem. Res. 13, 249–256
2 Amesz, J. (1983) Biochim. Biophys. Acta 726, 1–12
3 Kok, B., Forbush, B. and McGloin, M. (1971) Photochem. Photobiol. 14, 307–321
4 Cheniae, G.M. (1970) Annu. Rev. Plant Physiol. 21, 467–498
5 Dismukes, G.C. and Siderer, Y. (1981) Proc. Natl. Acad. Sci. USA 78, 274–278
6 Hansson, Ö. and Andréasson, L.-E. (1982) Biochim. Biophys. Acta 679, 261–268

7 Dismukes, G.C., Ferris, K. and Watnick, P. (1982) Photobiochem. Photobiophys. 3, 243–256
8 Cooper, S.R., Dismukes, G.C., Klein, M.P. and Calvin, M. (1978) J. Am. Chem. Soc. 100, 7248–7252
9 Brudvig, G.W., Casey, J.L. and Sauer, K. (1983) Biochim. Biophys. Acta 723, 366–371
10 Blankenship, R.E. and Sauer, K. (1974) Biochim. Biophys. Acta 357, 252–266
11 Goodin, D.B., Yachandra, V.K., Britt, R.D., Sauer, K. and Klein, M.P. (1984) Biochim. Biophys. Acta 767, 209–216
12 Goodin, D.B., Yachandra, V.K., Guiles, R.D., Britt, R.D., McDermott, A., Sauer, K. and Klein, M.P. (1984) in EXAFS and Near Edge Structure III (Hodgson, K.O., Hedman, B. and Penner-Hahn, J.E., eds.), pp. 130–135, Springer-Verlag, New York
13 Kirby, J.A., Robertson, A.S., Smith, J.P., Thompson, A.C., Cooper, S.R. and Klein, M.P. (1981) J. Am. Chem. Soc. 103, 5529–5537
14 Cheniae, G.M. and Martin, I.F. (1970) Biochim. Biophys. Acta 197, 219–239
15 Sayers, D.E., Lytle, F.W. and Stern, E.W. (1971) Phys. Rev. Lett. 27, 1204–1207
16 Eisenberger, P. and Kincaid, B.M. (1978) Science 200, 1441–1447
17 Powers, L. (1982) Biochim. Biophys. Acta 683, 1–38
18 Izawa, S., Heath, R.L. and Hind, G. (1969) Biochim. Biophys. Acta 180, 388–398
19 Kelley, P.M. and Izawa, S. (1978) Biochim. Biophys. Acta 502, 198–210
20 Kelley, P.M. and Izawa, S. (1979) Biophys. J. 25, 50a
21 Muallem, A. and Izawa, S. (1980) FEBS Lett. 115, 49–53
22 Izawa, S., Muallem, A. and Ramaswamy, N.K. (1983) in The Oxygen Evolving System of Photosynthesis (Inoue, Y., Crofts, A.R. Govindjee, Murata, N., Renger, G. and Satoh, K., eds.), pp. 293–302, Academic Press, Japan, Tokyo
23 Govindjee, Baianu, I.C., Critchley, C. and Gutowsky, H.S. (1983) in The Oxygen Evolving System of Photosynthesis (Inoue, Y., Crofts, A.R., Govindjee, Murata, N., Renger, G. and Satoh, K., eds.), pp. 305–315, Academic Press Japan, Tokyo
24 Sandusky, P.O. and Yocum, C.F. (1983) FEBS Lett. 162, 339–343
25 Yachandra, V.K., Guiles, R.D., Sauer, K. and Klein, M.P. (1986) Biochim. Biophys. Acta 850, 333–342
26 Kuwabara, T. and Murata, N. (1982) Plant Cell Physiol. 23, 533–539
27 Berthold, D.A., Babcock, G.T. and Yocum, C.F. (1981) FEBS Lett. 134, 231–234
28 Jaklevic, J., Kirby, J.A., Klein, M.P., Robertson, A.S., Brown, G.S. and Eisenberger, P. (1977) Solid State Commun. 23, 679–682
29 Powers, L., Chance, B., Ching, Y. and Angiolillo, P. (1981) Biophys. J. 34, 465–498
30 Stern, E.A. and Heald, S.M. (1979) Rev. Sci. Instrum. 50, 1579–1582
31 Goodin, D.B. (1983) Ph. D. Dissertation, University of California, Berkeley, CA, USA, Lawrence Berkely Laboratory Report, LBL-16901
32 Stern, E.A. (1974) Phys. Rev. B10, 3027–3037
33 Ashley, C.A. and Doniach, S. (1975) 11, 1279–1288
34 Teo, B.-K. and Lee, P.A. (1979) J. Am. Chem. Soc. 101, 2815–2832
35 Plaksin, P.M., Stoufer, R.C., Mathew, M. and Palenik, G.J. (1972) J. Am. Chem. Soc. 94, 2121–2122
36 Yachandra, V.K., Powers, L. and Spiro, T.G. (1983) J. Am. Chem. Soc. 105, 6596–6604
37 Co, M.S., Scott, R.A. and Hodgson, K.O. (1981) J. Am. Chem. Soc. 103, 986–988
38 Kirby, J.A. (1981) Ph.D. Dissertation, University of California, Berkeley, CA, USA, Lawrence Berkeley Laboratory Report, LBL-12705
39 Eisenberger, P. and Lengeler, B. (1980) Phys. Rev. B22, 3551–3562
40 Chen, B.M. (1970) Ph.D. Dissertation, Michigan State University, MI, USA
41 Kirner, J.F. and Scheidt, W.R. (1975) Inorg. Chem. 14, 2081–2086
42 Cammarata, K., Tamura, N., Sayre, R. and Cheniae, G. (1984) in Advances in Photosynthesis Research (Sybesma, C., Ed.), Vol. I, pp. 311–320, Martinus Nijhoff/Dr. W. Junk Publishers, Dordrecht, The Netherlands
43 Kuwabara, T. and Murata, N. (1983) Plant Cell Physiol. 24, 741–747
44 Ghanotakis, D.F., Babcock, G.T. and Yocum, C.F. (1984) Biochim. Biophys. Acta 765, 388–398
45 Kirby, J.A., Goodin, D.B., Wyrdrzynski, T., Robertson, A.S. and Klein, M.P. (1981) J. Am. Chem. Soc. 103, 5537–5542
46 Shulman, R.G., Yafet, Y., Eisenberger, P. and Blumberg, W.E. (1976) Proc. Natl. Acad. Sci. USA 73, 1384–1388
47 Roe, A.L., Schneider, D.J., Mayer, R.J., Pyrz, J.W., Widom, J. and Que, Jr., L. (1984) J. Am. Chem. Soc. 106, 1676–1681
48 De Paula, J.C. and Brudvig, G.W. (1985) J. Am. Chem. Soc. 107, 2643–2648
49 Van Gorkom, H.J. (1985) Photosyn. Res. 6, 97–112